

This article was downloaded by: [Rutgers University], [Tao Wan]

On: 12 August 2011, At: 07:20

Publisher: Taylor & Francis

Informa Ltd Registered in England and Wales Registered Number: 1072954 Registered office: Mortimer House, 37-41 Mortimer Street, London W1T 3JH, UK

International Journal of Computer Mathematics

Publication details, including instructions for authors and subscription information:

<http://www.tandfonline.com/loi/gcom20>

An application of compressive sensing for image fusion

Tao Wan^a & Zengchang Qin^{a b}

^a Robotics Institute, Carnegie Mellon University, Pittsburgh, USA

^b Intelligent Computing and Machine Learning Lab, School of Automation Science & Electrical Engineering, Beihang University, Beijing, 100191, China

Available online: 12 Aug 2011

To cite this article: Tao Wan & Zengchang Qin (2011): An application of compressive sensing for image fusion, International Journal of Computer Mathematics, DOI:10.1080/00207160.2011.598229

To link to this article: <http://dx.doi.org/10.1080/00207160.2011.598229>



PLEASE SCROLL DOWN FOR ARTICLE

Full terms and conditions of use: <http://www.tandfonline.com/page/terms-and-conditions>

This article may be used for research, teaching and private study purposes. Any substantial or systematic reproduction, re-distribution, re-selling, loan, sub-licensing, systematic supply or distribution in any form to anyone is expressly forbidden.

The publisher does not give any warranty express or implied or make any representation that the contents will be complete or accurate or up to date. The accuracy of any instructions, formulae and drug doses should be independently verified with primary sources. The publisher shall not be liable for any loss, actions, claims, proceedings, demand or costs or damages whatsoever or howsoever caused arising directly or indirectly in connection with or arising out of the use of this material.

An application of compressive sensing for image fusion

Tao Wan^{a*} and Zengchang Qin^{a,b}

^aRobotics Institute, Carnegie Mellon University, Pittsburgh, USA; ^bIntelligent Computing and Machine Learning Lab, School of Automation Science & Electrical Engineering, Beihang University, Beijing 100191, China

(Received 30 November 2010; revised version received 3 March 2011; accepted 13 April 2011)

Compressive sensing (CS) has inspired significant interests because of its compressive capability and lack of complexity on the sensor side. This paper introduces a novel framework of image fusion based on the CS principle. First, we present a study of three sampling patterns and investigate their performance on CS reconstruction. We then propose a novel image fusion algorithm by using an improved sampling pattern. Finally, the CS-based image fusion approach is applied to various image modalities and evaluated both visually and in terms of fusion quality metrics. The simulations demonstrate that CS-based image fusion has a number of perceived advantages in comparison with image fusion in the multiresolution (MR) domain, providing a truly different and more advanced way for fusing multimodality images.

Keywords: compressive sensing; CS-based image fusion; multiresolution image fusion

2010 AMS Subject Classification: 68U10

1. Introduction and motivation

Image fusion aims to combining the complementary information from two or more images into a single image to provide more informative form than any of the input images [31,32]. For example, the infrared (IR) and visible images are two common image modalities. IR image is captured by image sensor which is sensitive to IR light with low definition. On the contrary, visible image has high definition with more details of the scene. Thus, the appropriate fusion of IR and visible images can obtain a better representation of the environmental condition to aid human visual perception [13]. Another important application of image fusion is utilized in the medical diagnostics and treatment, in which the pre-registered patient images from the same or multiple modalities are merged in order to provide additional diagnostic information [35].

Image fusion methods can be broadly classified into two categories [8]. The spatial domain fusion approaches generally produce spatial distortion in the fused image which becomes a negative factor in the subsequent processing tasks. This disadvantage can be well handled by transform domain approaches. Among them, multiresolution (MR) decomposition schemes recently become popular for fusing remote sensing images [19]. These fusion methods include

*Corresponding author. Email: tao.wan.wan@gmail.com

Laplacian pyramid-based [34], curvelet transform [17], wavelet transform [15,29,32], etc. In general, wavelet-based approaches outperform the other methods. All these methods require knowledge of the original images. A natural question emerges about the possibility of fusing images without acquiring the original input images. The theory of compressive sensing (CS) [5,9] or compressive sampling offers a feasible way to collect samples without assuming any prior information about the signal being observed, thereby it motivates our research on image fusion using CS.

In the previous work, Wan *et al.* [30] introduced a new concept of compressive image fusion. The main purpose of this work was to explore the properties of compressive sensing technique and their potential use in image fusion. However, there are still many issues that remain unsolved. For instance, apart from the different sampling patterns, are there any other factors that could influence the performance of the compressive sensing reconstruction? And what happens when more than 50% compressive measurements are used in both compressive reconstruction and image fusion? In this paper, these questions are studied and analysed for finding the answers. Therefore, the research presented here significantly enhances and expands our previous work [30] with an improved algorithm and more complementary discussions regarding the compressive image fusion.

The remainder of the paper is organized as follows. Section 2 provides a brief description on CS and introduces new sampling patterns with their performance on the CS reconstruction. In Section 3, a new CS-based image fusion algorithm is developed in comparison with a conventional image fusion technique in the MR domain. Simulation results and discussions are presented in Section 4. Finally, conclusions and suggestions for future work are given in Section 5.

2. Sampling patterns in compressive sensing

The recently developed theory of CS demonstrated that sparse or compressible signals can be accurately reconstructed from a small set of incoherent projections, which is far fewer than the number of samples if the signal is sampled at the Nyquist rate, thus significantly reducing the sampling and computation costs [5,9]. For this reason, CS has many promising applications in data compression [2,4], image acquisition [7,10] and medical imaging [21,25]. In this work, we investigate its potential application in the image fusion. We first provide a brief introduction to CS and investigate the impact of different sampling patterns on the CS reconstruction.

2.1 Background on compressive sensing

The Shannon sampling theorem specifies that signals, images, videos and other data can be exactly recovered from a set of uniformly spaced samples taken at the Nyquist rate of twice the highest frequency present in the signal of interest [22]. The Nyquist rate is so high that too many samples result, making compression a necessity prior to storage or transmission. The traditional image compression method convert high-resolution images into a relatively small bit streams, in effect turning a large digital data set into a substantially smaller one. This procedure is inefficient, since a large number of acquired samples ends up being discarded [1].

CS is a new method to capture and represent compressible signals at a rate significantly below the Nyquist rate, which employs non-adaptive linear projections that contain sufficient information to effectively perform a certain image processing task. Hence, it has a simplicity in hardware implementation and a reduction in computation cost.

To begin with, we consider a real-valued, finite-length, one-dimensional signal¹ $\mathbf{x} \in \mathbb{R}^N$ with elements $x[n], n = 1, 2, \dots, N$. The signal is K -sparse if it can be represented as:

$$\mathbf{x} = \Psi\boldsymbol{\theta}, \tag{1}$$

where Ψ is some basis and θ is a vector containing only $K \ll N$ nonzero coefficients. θ can be thought of as \mathbf{x} in domain Ψ . Based on the terms of CS, the signal \mathbf{x} can be recovered from $M = c \cdot K$ fixed non-adaptive linear projects onto a second basis, called the measurement basis, and where $c > 1$ is a small over-measuring constant. The compressive measurements can be computed as:

$$\mathbf{y} = \Phi \mathbf{x}, \quad (2)$$

where $\mathbf{y} \in \mathbb{R}^M$ and Φ is an $M \times N$ matrix representing the measurement process. Although $M < N$ makes the recovery of the signal \mathbf{x} from the measurements \mathbf{y} ill-posed in general, recent CS experiments show that the recovery is possible and practical by adding assumption of signal sparsity [26].

2.2 Sampling patterns in CS measurement

According to the CS theory, the recovery of original signal can be obtained through a reconstruction algorithm using the compressive measurements \mathbf{y} , which are obtained from a non-adaptive linear projection of the signal onto a random measurement basis matrix Φ . Thereby, the way of extracting the CS measurements will affect the final reconstruction process. There are different ensembles of CS matrices defined in previous CS literature [5,9,26]. For example, a toolbox called *l1-magic* [3] used a two-dimensional fast Fourier transform and the CS matrix Φ was constructed by a star-shaped sampling pattern in the two-dimensional Fourier plane, as shown in Figure 1(a). The white lines indicate the locations of the frequencies that are used to compute compressive measurements \mathbf{y} . Due to the special structure of the Fourier transform underlying the partial Fourier ensemble, we design two new sampling patterns named ‘double-star’ and ‘star-circle’ [30]. They are shown in Figure 1(b) and 1(c), respectively. The reason of selecting more coefficients at the centre of the transform plane is that images usually have much more meaningful low-frequency information

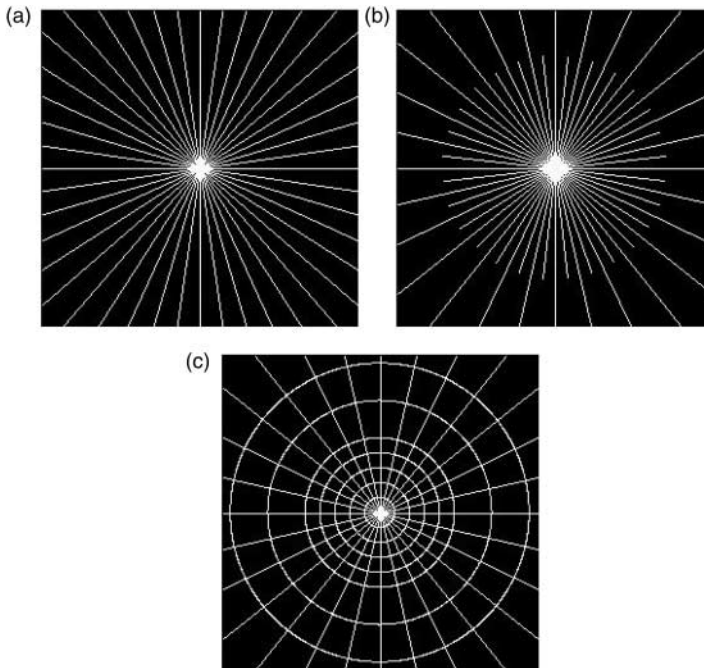


Figure 1. Sampling patterns. (a) Star shape. (b) Double-star shape. (c) Star-circle shape.

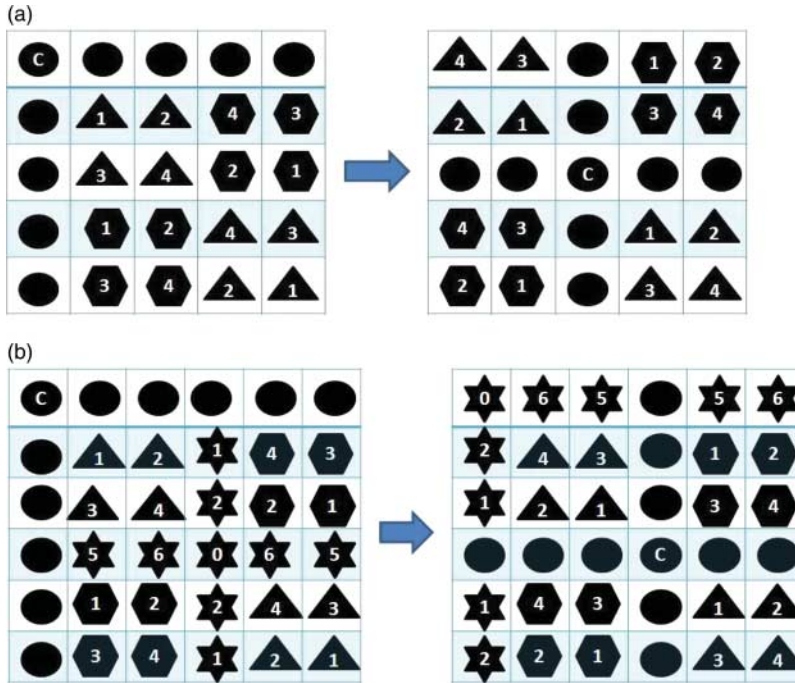


Figure 2. Improved star-shaped sampling pattern. (a) Odd-dimensional case. (b) Even-dimensional case.

comparing with high-frequency information, so the white lines are chosen with higher density sampling at low frequency to encode more features of source images. By changing the density of lines in the sampling patterns, we can obtain different numbers of measurements.

In the l_1 -magic toolbox, the sampling method by using the star-shaped pattern can only process the image with length of 2^n . In our experiments, we make an improvement by applying this pattern to the images with any lengths. Two examples for odd- and even-dimensional patterns are displayed in Figure 2(a) and 2(b), respectively. In each case, the pattern is divided into four centrosymmetric patches. They are shifted after the Fourier transform and the top left frequency component is moved from the original position to the centre of the pattern. For the pattern with both odd and even dimensions, we add one extra row of zeros to make odd to even.

All three patterns illustrated in Figure 1 are tested on various types of images, including 40 natural images [24], 35 IR and 35 visible images captured by the digital cameras [23]. These surveillance images are also used in the following image fusion experiments. Figure 3 presents the peak signal-to-noise ratio (PSNR) of the recovered images for these three sampling patterns. The M/N on the x -axis is the rate of the CS measurements over the original signal. Figure 3(a), (c) and (e) are the partial results using up to 55% measurements for a better visual observation. The figure shows that better quality images can be obtained by simply taking more measurements because the CS measurement process is progressive. In these three cases, the double-star-shaped pattern yields the best performance in all types of images in terms of the PSNR values. We also note that the reconstruction process demands less computation time by using the double-star-shaped pattern. The reason is because this sampling pattern makes a good balance of choosing the low and high frequencies in the Fourier domain.

Moreover, curves of visible and IR images appear to be flat as a high proportion of the measurements are used for the reconstruction. This is because that the PSNR value is not available when the reconstruction algorithm ideally generates a restored image that is identical to the original

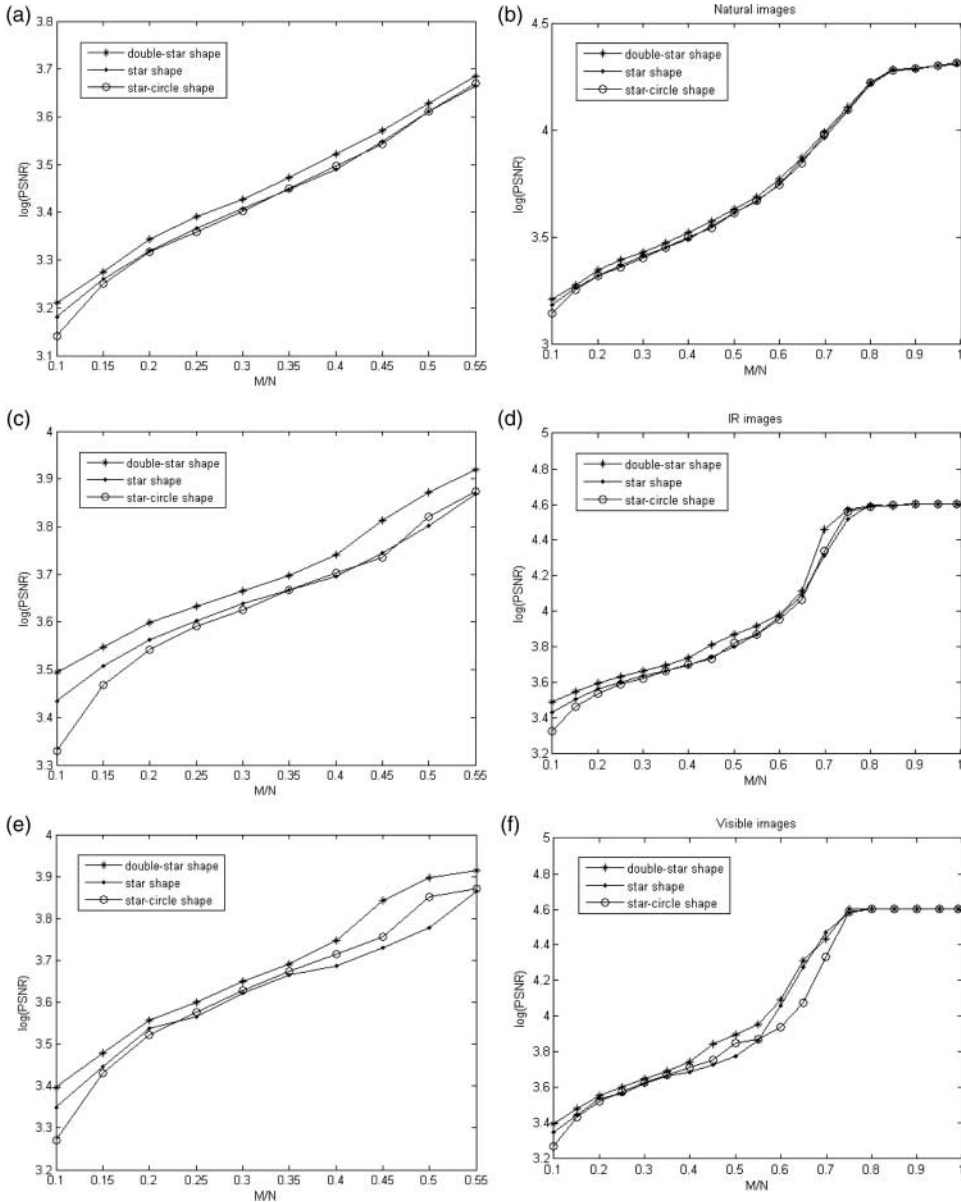


Figure 3. Log values of PSNR for reconstructions of a variety of images. (a) Natural images ($M/N : 0.1-0.55$). (b) Natural images ($M/N : 0.1-1.0$). (c) IR images ($M/N : 0.1-0.55$). (d) IR images ($M/N : 0.1-1.0$). (e) Visible images ($M/N : 0.1-0.55$). (f) Visible images ($M/N : 0.1-1.0$).

input image. In this case, we assume that the reconstructed image has 100 dB of PSNR (i.e. $\log(100) = 4.61$) since the image estimated can hardly be distinguished from the original at a PSNR of about 60 dB [11]. However, the experimental results show that natural images do not lead to a perfect reconstruction even by entailing more measurements. Additionally, there is a notable difference between natural images and visible and IR images in that the latter two types of images achieve a better PSNR with the same or fewer CS measurements. This can be explained using Figure 4 which is a typical example showing the plotted histograms corresponding to these three types of images. The standard deviation is used here to measure the dispersion of the grayscale

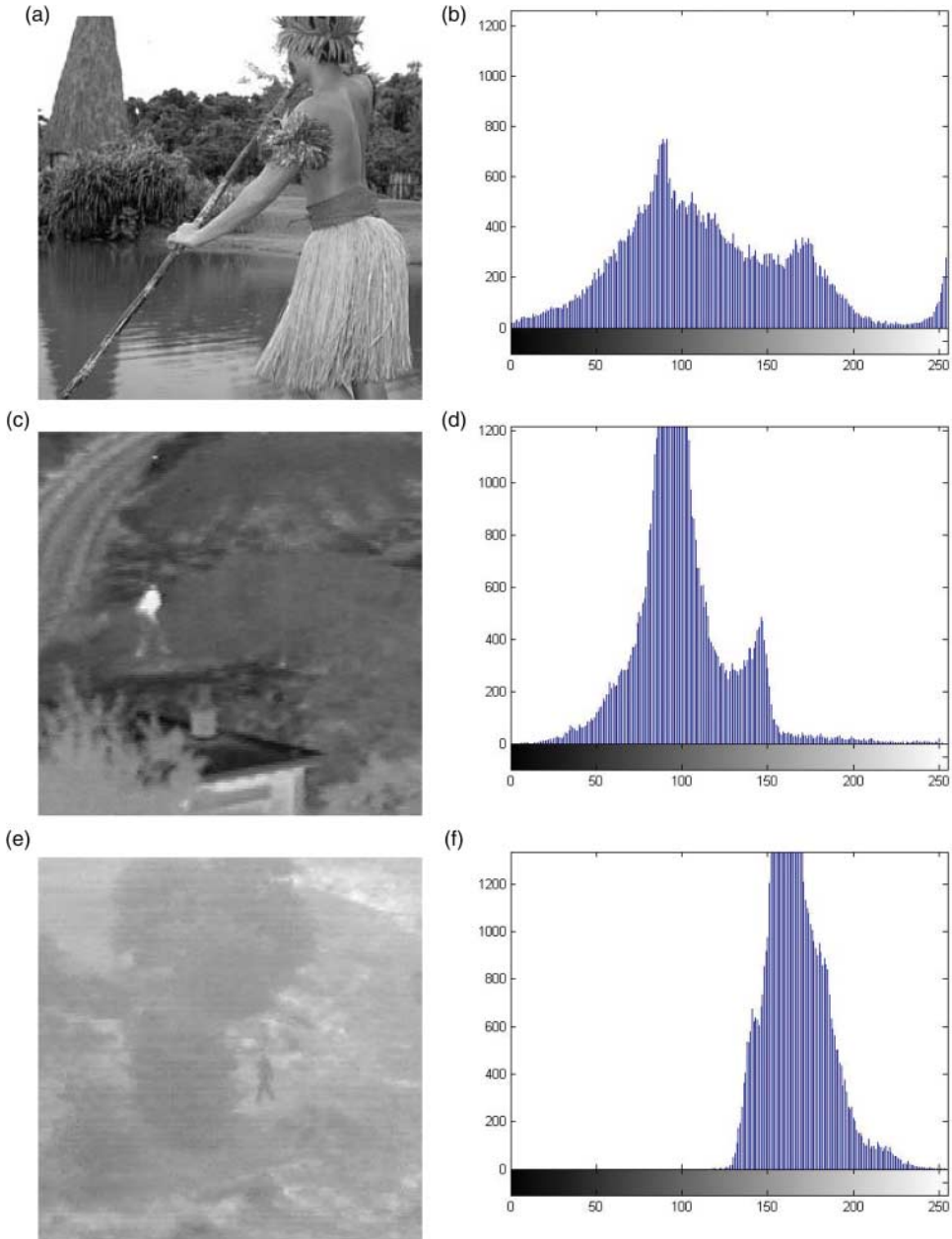


Figure 4. Histograms of greyscale distributions for three images. (a) A natural image. (b) Histogram for the natural image (the standard deviation is $\sigma = 62.66$). (c) An IR image. (d) Histogram for the IR image (the standard deviation is $\sigma = 26.57$). (e) A visible image. (f) Histogram for the visible image (the standard deviation is $\sigma = 17.85$). The greyscale values are measured on a 0–255 scale.

image data. The real signal of the natural image tends to be less sparse than the visible and IR images. We know that signal sparsity is one of the important assumptions adopted in the CS reconstruction. Thus, natural images require more CS measurements to achieve a desirable threshold of PSNR (i.e., 60 dB or $\log(60) = 4.09$) or fail to reach this value for some particular images. It is sensible to apply the CS technique to multisensor images.

3. Compressive image fusion

There is, to our knowledge, little research regarding the applicability of CS to image fusion in literature [28,30]. The centre piece of this work is to develop a new image fusion algorithm making good use of CS technique. We start with classic image fusion methods using MR decompositions.

3.1 Image fusion in the multiresolution domain

As previously mentioned in Section 1, MR decomposition is a very useful tool for analyzing images. Among the various frameworks in which image fusion has been formulated, the MR method has been one of the most intensively studied and used in practice. An MR scheme decomposes the signal in a hierarchical manner where each level corresponds to a reduced-resolution approximation. MR fusion approaches are very important for many reasons: (i) MR representations enable one to consider and fuse image features separately at different scales; (ii) They produce large coefficients near edges, thus revealing salient information [16]; (iii) MR methods have been approved to be efficient and robust [19]. In past decades, wavelets have emerged as an effective tool for this problem due to their energy compaction property [29,31,34]. In this paper, we address the image fusion problem in the context of wavelet transforms.

The basic idea underlying the wavelet-based image fusion approach is to perform a wavelet decomposition on each source image. Some specific fusion rules are applied to construct a composite representation from these inputs. The fused image is obtained by taking an inverse wavelet transform. As our main focus is not on MR image fusion, we choose a simple maximum selection (MS) fusion scheme to fuse the input images at the pixel level. MS is a widely used fusion rule which considers the maximum absolute values of the wavelet coefficients from the source images as the fused coefficients.

We process the detailed wavelet coefficients and approximation images in different ways. First, the detailed wavelet coefficients are composed using the MS fusion rule:

$$D_F = D_M \quad \text{with} \quad M = \arg \max_{i=1, \dots, I} (|D_i|), \quad (3)$$

where D_F are the composite coefficients, D_M is the maximum absolute value of the input wavelet coefficients, and I the total number of the source images. The fused approximation image A_F is constructed by:

$$A_F = \frac{1}{I} \sum_{i=1}^I (A_i). \quad (4)$$

As we can see, an image fusion approach based on wavelets requires to manipulate detailed coefficients and approximation images, while in the compressive domain, it only considers the compressive measurements.

3.2 Image fusion in the compressive domain

In this section, we formulate an image fusion algorithm that uses compressive measurements to fuse multiple images into a single representation. Recent theoretical results show that when the signal is sparse or nearly sparse in some basis, then with high probability, the measurements essentially encode the salient information in the signal. Further, the unknown signal can be estimated from these compressive measurements to within a controllable mean-squared error [5,9]. In this sense, we can apply a similar fusion scheme to that used in the wavelet domain in the compressive domain, so the difference is that image fusion is performed on the compressive measurements

Table 1. Compressive image fusion algorithm.

Algorithm: Compressive image fusion

1. Take the compressive measurements $Y_i, i = 1, \dots, I$ for the i th input image using the double-star-shaped sampling pattern.
2. Calculate the fused measurements using the formula: $Y_F = Y_M$ with $M = \arg \max_{i=1, \dots, I} (|Y_i|)$.
3. Reconstruct the fused image from the composite measurements Y_F via the total variation optimization method [5,6].

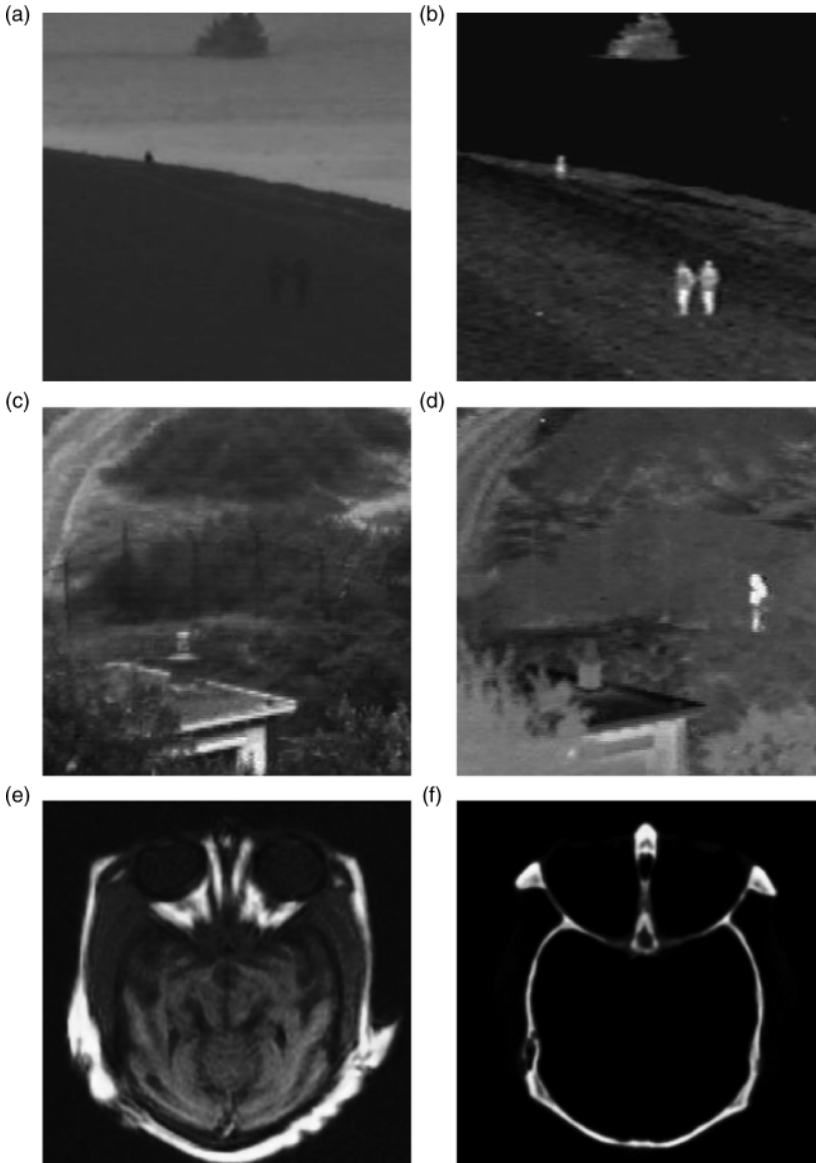


Figure 5. Experimental images. (a) 256×256 'Kayak' visible image. (b) 256×256 'Kayak' IR image. (c) 256×256 'UN Camp' visible image. (d) 256×256 'UN Camp' IR image. (e) 256×256 MRI image. (f) 256×256 CT image.

rather than on the wavelet coefficients. The basic steps are described in Table 1. The fused image is recovered via a total variation optimization presented in [5].

There is a significant number of CS literature focusing on problems in signal reconstruction and image approximation. For instance, one technique employs a specialized interior-point method for solving CS reconstruction in which a preconditioned conjugate gradient method is used to compute the search step [12]. These methods generally rely on nonlinear recovery algorithms based on convex optimization and signals can be recovered from what appear to be highly incomplete data. Among them, *l1-magic* [3] based on the methodology proposed in [5] achieves robust and reliable reconstructed results, particularly for signals that are not strictly sparse. Our CS-based fusion algorithm adopts this reconstruction method to restore the resultant fused images. One drawback of this method is the high computational complexity.

4. Simulation results and discussions

Objective evaluation criteria are applied to compare fusion results obtained using different sampling patterns. Since ground-truth data are not available here, Piella's [20] and Petrovic's [18] metrics are used to measure the relative amount of salient information conveyed in the fused image. Piella's quality assessment algorithm evaluates the quality of fused images, which assumes that in local regions the fused image should resemble whichever source image is the most salient. It is based on a recently introduced image quality index by Wang and Bovik [33]. The complete fusion quality measure is defined as:

$$Q_E(A, B, F) = Q_w(A, B, F) \cdot Q_w(A', B', F')^\alpha, \quad (5)$$

where A and B are the input images, F is the fused image, $Q_w(A, B, F)$ is a quality metric over a pre-specified window defined in [20], and $Q_w(A', B', F')$ is the same measure computed with the edge images (A', B', F') , α is a parameter that expresses the contribution of the edge image compared to the original images. As with Piella's metric, Petrovic's assessment method does not require a reference image that is ideal for the realistic use. The detailed implementation is described in [18]. It should be noted that this method aims to objectively measure the performance of a given pixel-level image fusion system, therefore the visual information is associated with the edge information while the region information is ignored.

Three pairs of images shown in Figure 5 are used in the experiments. We discover that the quality of the reconstruction results are increased by quantizing the original signal with respect to the PSNR values. Figure 6 shows the reconstruction results obtained using the Lloyd's algorithm

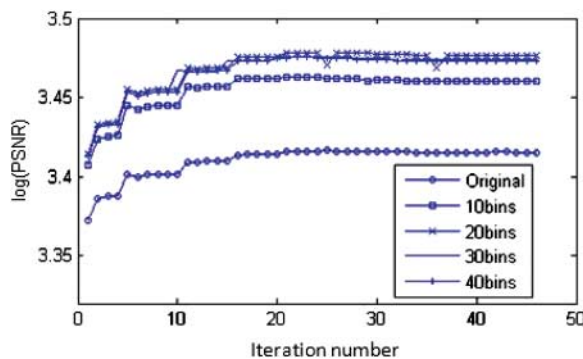


Figure 6. Log values of PSNR for reconstructions of 'Kayak' IR image.

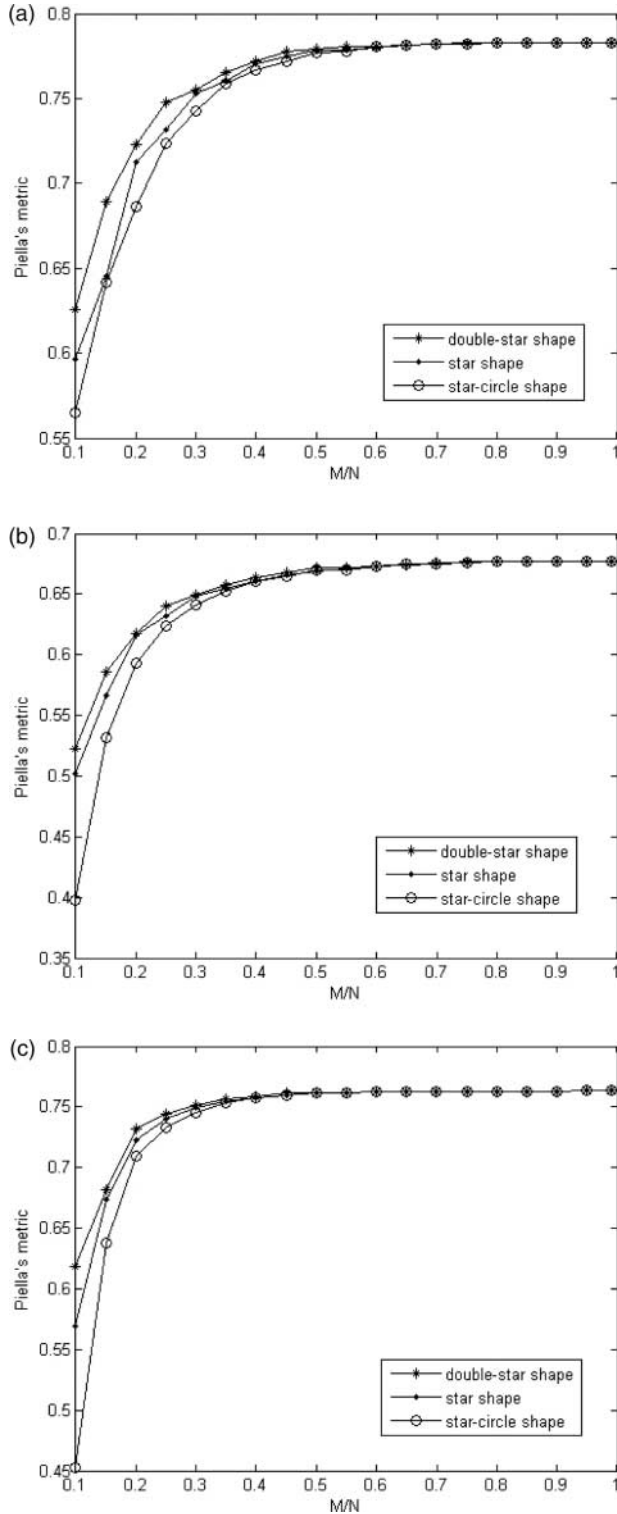


Figure 7. Piella's metric results using different sampling patterns for different images. (a) 'Kayak' images. (b) 'UN Camp' images. (c) Medical images.

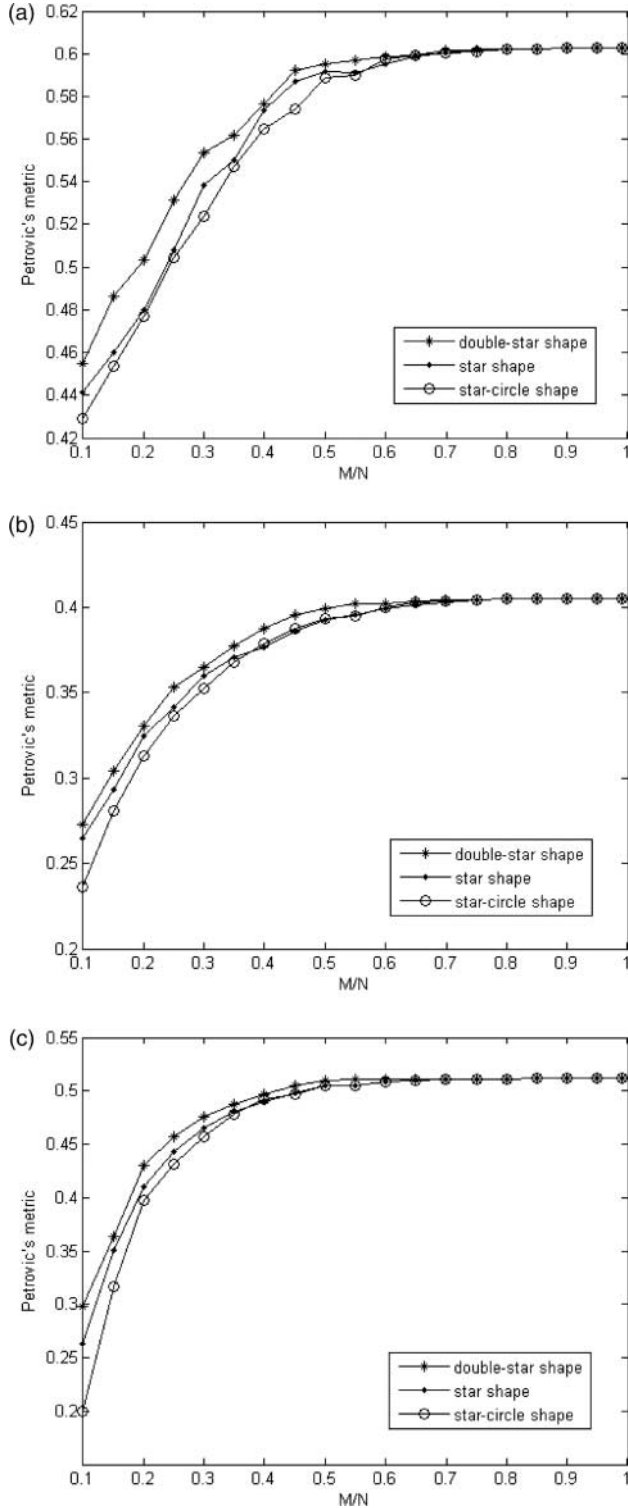


Figure 8. Petrovic's metric results using different sampling patterns for different images. (a) 'Kayak' images. (b) 'UN Camp' images. (c) Medical images.

Downloaded by [Rutgers University], [Tao Wan] at 07:20 12 August 2011

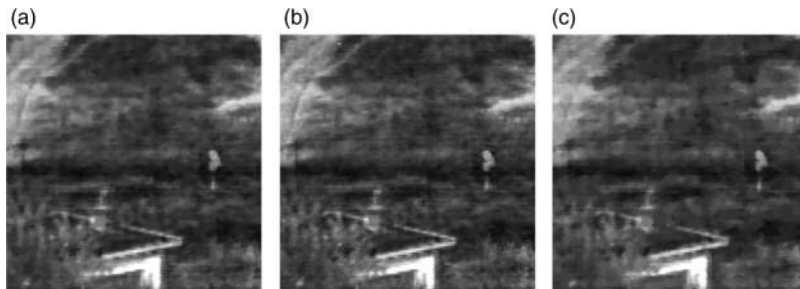


Figure 9. Fusion results for ‘UN Camp’ images using different sampling patterns with 30% compressive measurements. (a) Star shape. (b) Double-star shape. (c) Star-circle shape.

[14] in comparison with the ones yielded without quantization. A better reconstruction result is achieved by increasing the number of quantization bins. In our experiments, the quantization method is not applied to the source images since the details of each input image need to be maintained in the fusion process.

In Figures 7 and 8, we present some results of the proposed image fusion algorithm applied to these test images using Piella’s and Petrovic’s metrics, respectively. There is a clear performance improvement by using the double-star-shaped sampling pattern over the other two patterns when fewer measurements are used. This can also be confirmed from the visual examination in Figure 9 in which the fused image produced by double-star shape maintains better detailed background using 30% compressive measurements. However, all three patterns yield similar results as the number of the compressive measurements increases. The shape of the plotted polylines demonstrates that the two metrics generally offer correlated fusion assessment results. We note that by using nearly 50% fewer compressive measurements than reconstructed pixels, we can achieve almost the same fusion results as using the entire set of pixels. The numeric results of these two quality metrics obtained using the double-star sampling pattern are listed in Tables 2 and 3. Figure 10(a)–(e) illustrate the fusion results using 10%, 25%, 50%, 75%, and all Fourier coefficients as the compressive measurements. The original input images are presented in Figure 5(a) and 5(b). It indicates that there is no perceivable difference between the fused images using the measurements over 50% of Fourier coefficients.

Table 2. Performance comparisons using Piella’s metric [20] using the double-star pattern.

Example	M/N								
	0.1	0.2	0.3	0.4	0.5	0.6	0.7	0.8	0.9
‘Kayak’ images	0.6256	0.7229	0.7551	0.7719	0.7792	0.7808	0.7822	0.7828	0.7830
‘UN Camp’ images	0.5221	0.6172	0.6490	0.6642	0.6717	0.6733	0.6759	0.6768	0.6773
Medical images	0.6179	0.7315	0.7515	0.7589	0.7617	0.7623	0.7628	0.7630	0.7632

Table 3. Performance comparisons using Petrovic’s metric [18] using the double-star pattern.

Example	M/N								
	0.1	0.2	0.3	0.4	0.5	0.6	0.7	0.8	0.9
‘Kayak’ images	0.4546	0.5034	0.5537	0.5767	0.5950	0.5986	0.6017	0.6022	0.6025
‘UN Camp’ images	0.2725	0.3302	0.3645	0.3871	0.3991	0.4020	0.4044	0.4048	0.4050
Medical images	0.2978	0.4306	0.4760	0.4965	0.5059	0.5109	0.5110	0.5113	0.5116

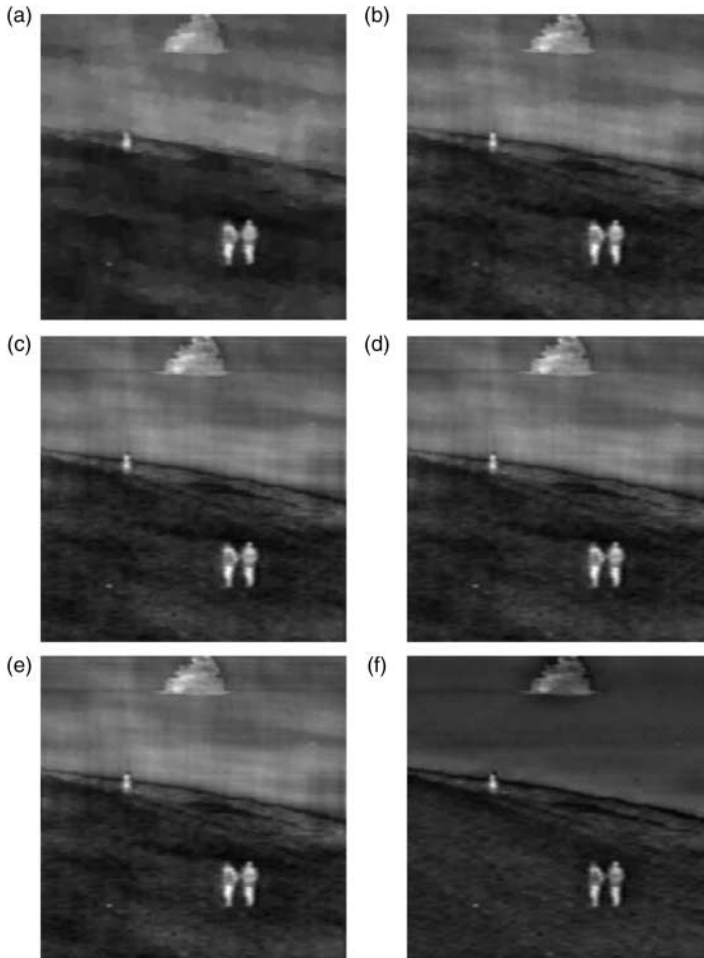


Figure 10. Fusion results (The double-star-shaped sampling pattern is used here in the compressive image fusion algorithm). (a) Fused image recovered from $M = 6554$ compressive measurements ($M/N = 0.10$). (b) Fused image recovered from $M = 16384$ compressive measurements ($M/N = 0.25$). (c) Fused image recovered from $M = 32768$ compressive measurements ($M/N = 0.50$). (d) Fused image recovered from $M = 49152$ compressive measurements ($M/N = 0.75$). (e) Fused image using all Fourier coefficients ($N = 65536$). (f) Fused image using a MS scheme in the wavelet domain.

Furthermore, compared with the fused image shown in Figure 10(f) that is obtained by using a MS scheme in a complex wavelet domain, our proposed fusion algorithm does not provide a comparable result in terms of human perception. The poor image quality is mainly due to the fact that Fourier coefficients have their own limitations as compressive measurements to be used in image fusion. This has been proved by observing Figure 10(e). The reconstruction algorithm should also be accounted for in this case since the method was originally applied to one single image rather than multiple images. Figure 11 displays more fusion results in comparison with the wavelet-based fusion scheme.

Although the obtained fusion results are not perfect, CS-based image fusion has a number of advantages over conventional image fusion algorithms. It offers computational and storage savings by using a CS technique. Compressive measurements are progressive in the sense that larger numbers of measurements will lead to higher quality reconstructed images. Image fusion can be performed without acquiring the observed signals. Additionally, the recently proposed

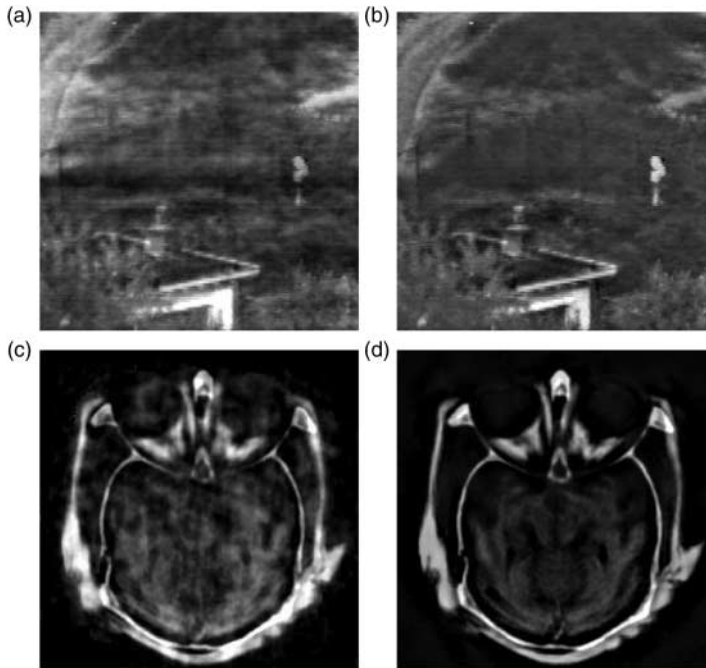


Figure 11. More fusion results for ‘UN Camp’ and medical images. From left to right, fused image recovered from $M/N = 0.5$, and fused image using a MS scheme in the wavelet domain.

compressive imaging system [10,27], which relies on a single photon detector, enables imaging at new wavelengths inaccessible or prohibitively expensive using current focal plane imaging arrays. The development of this new imaging system has motivated investigation into CS-based image fusion techniques for practical use. This will significantly reduce the hardware cost, meanwhile expand image fusion in modern military and civilian imaging applications in a cheaper and more efficient way. However, the compressive measurements lose spatial information due to the CS measurement process. Therefore, traditional image fusion rules operating on local knowledge cannot be applied to compressive image fusion.

5. Conclusions and future work

In this paper, we have presented a new image fusion algorithm in the compressive domain, in which three sampling patterns were investigated for reconstruction from compressive samples. One key advantage offered by this newly introduced technique is that samples can be collected without assuming any prior information about the signal being observed. Therefore, compressive image fusion provides a truly different way of fusing images compared with traditional fusion methods at pixel or feature level. Apart from computational and storage savings by using CS techniques, CS-based image fusion has a number of advantages over conventional image fusion algorithms. Most importantly, the recently developed compressive imaging system makes it promising to expand compressive image fusion in modern military and civilian imaging applications.

As we previously stated, the main weakness of compressive image fusion is that spatial information is lost due to compressive sensing measurement process. Consequently, conventional window-based fusion schemes cannot be applied to a CS-based fusion algorithm. By examining the underlying structure of the compressive measurements, a new fusion strategy could be derived in future work.

Acknowledgement

This work is partially funded by the NCET of MOE, China Scholar Council and the SRF for ROCS, SEM.

Note

1. An image can be vectorized into a long one-dimensional vector.

References

- [1] A. Achim, B. Buxton, G. Tzagkarakis, and P. Tsakalides, *Compressive sensing for ultrasound rf echoes using α -stable distributions*, Proceedings of the IEEE Conference on Engineering in Medicine and Biology Society, Buenos Aires, Argentina, 2010, pp. 4304–4307.
- [2] M. Akcakaya and V. Tarokh, *A frame construction and a universal distortion bound for sparse representations*, IEEE Trans. Signal Process. 56(6) (2008), pp. 2443–2450.
- [3] E. Candès and J. Romberg, *l1-magic: Recovery of sparse signal via convex programming*, Code package available at <http://www.l1-magic.org>.
- [4] E. Candès and T. Tao, *Decoding by linear programming*, IEEE Trans. Inform. Theory 51(12) (2005), pp. 4203–4215.
- [5] E. Candès, J. Romberg, and T. Tao, *Robust uncertainty principles: Exact signal reconstruction from highly incomplete frequency information*, IEEE Trans. Inform. Theory 56(2) (2006), pp. 489–509.
- [6] E. Candès, J. Romberg, and T. Tao, *Stable signal recovery from incomplete and inaccurate measurements*, Commun. Pure Appl. Math. 59(8) (2006), pp. 1207–1223.
- [7] W.L. Chan, M.L. Moraverc, R.G. Baraniuk, and D.M. Mittleman, *Terahertz imaging with compressed sensing and phase retrieval*, Opt. Lett. 33(9) (2008), pp. 974–976.
- [8] M. Deshmukh and U. Bhosale, *Image fusion and image quality assessment of fused images*, Int. J. Image Process. 4(5), p. 484.
- [9] D.L. Donoho, *Compressed sensing*, IEEE Trans. Inform. Theory 52(4) (2006), pp. 1289–1306.
- [10] M. Duarte, M. Davenport, D. Takhar, J. Laska, T. Sun, K. Kelly, and R. Baraniuk, *Single-pixel imaging via compressive sampling*, IEEE Signal Process. Mag. 25(2) (2008), pp. 83–91.
- [11] K. Egiazarian, A. Foi, and V. Katkovnik, *Compressed sensing image reconstruction via recursive spatially adaptive filtering*, Proceedings of the IEEE International Conference on Image Processing, San Antonio, Texas, USA, Vol. 1, 2007, pp. 549–552.
- [12] S.J. Kim, K. Koh, M. Lustig, and S. Boyd, *An efficient method for compressed sensing*, Proceedings of the IEEE International Conference on Image Processing, San Antonio, Texas, USA, Vol. 3, 2007, pp. 117–120.
- [13] X. Li and S. Qin, *Efficient fusion for infrared and visible images based on compressed sensing principle*, IET Image Process. 5(2) (2010), pp. 141–147.
- [14] S.P. Lloyd, *Least squares quantization in PCM*, IEEE Trans. Inform. Theory 28(2) (1982), pp. 129–137.
- [15] A. Loza, D. Bull, N. Canagarajah, and A. Achim, *Statistical model-based fusion of noisy images in the wavelet domain*, Comput. Vis. Image Understand. 114 (2010), pp. 54–65.
- [16] D. Marr, *Vision*, W. H. Freeman, New York, 1982.
- [17] F. Nencini, A. Garzelli, S. Baronti, and L. Alparone, *Remote sensing image fusion using the curvelet transform*, Inform. Fusion 8(2) (2007), pp. 143–156.
- [18] V. Petrovic and C. Xydeas, *On the effects of sensor noise in pixel-level image fusion performance*, Proceedings of the International Conference on Image Fusion, Paris, France, Vol. 2, 2000, pp. 14–19.
- [19] G. Piella, *A general framework for multiresolution image fusion: from pixels to regions*, Inform. Fusion 4 (2003), pp. 259–280.
- [20] G. Piella and H. Heijmans, *A new quality metric for image fusion*, Proceedings of the IEEE Conference on Image Processing, Barcelona, Spain, Vol. 2, 2003, pp. 173–176.
- [21] J. Provost and F. Lesage, *The application of compressed sensing for photo-acoustic tomography*, IEEE Trans. Med. Imag. 28(4) (2009), pp. 585–594.
- [22] C.E. Shannon, *Communication in the Presence of Noise*, Proc. IEEE 72 (1984), pp. 1192–1201.
- [23] The online resource for research in image fusion. Available at <http://www.imagefusion.org/>.
- [24] *The Berkeley Segmentation Dataset Benchmark*, University of California, Berkeley, CA. Available at <http://www.eecs.berkeley.edu/Research/Projects/CS-vision/grouping/segbench/>, Jul. 2003.
- [25] J. Trzasko and A. Manduca, *Highly undersampled magnetic resonance image reconstruction via homotopic l_0 -minimization*, IEEE Trans. Med. Imag. 28(1) (2009), pp. 106–121.
- [26] Y. Tsaig and D. L. Donoho, *Extensions of compressed sensing*, Signal Process. 86 (2005), pp. 549–571.
- [27] M.B. Wakin, J.N. Laska, M.F. Duarte, D. Baron, S. Sarvotham, D. Takhar, K.F. Kelly, and R.G. Baraniuk, *An architecture for compressive imaging*, Proceedings of the IEEE International Conference on Image Processing, Atlanta, Georgia, USA, 2006, pp. 1273–1276.
- [28] T. Wan and Z. Qin, *An application of compressive sensing for image fusion*, The ACM International Conference on Image and Video Retrieval, Xi'an, China, 2010, pp. 3–9.

- [29] T. Wan, N. Canagarajah, and A. Achim, *Region-based multisensor image fusion using generalized Gaussian distribution*, International Workshop on Nonlinear Signature and Image Processing, Bucharest, Romania, 2007.
- [30] T. Wan, N. Canagarajah, and A. Achim, *Compressive image fusion*, Proceedings of the IEEE International Conference Image Processing, San Diego, California, USA, 2008, pp. 1308–1311.
- [31] T. Wan, G. Tzagkarakis, P. Tsakalides, N. Canagarajah, and A. Achim, *Context enhancement through image fusion: A multiresolution approach based on convolution of cauchy distributions*, Proceedings of the IEEE Conference on Acoustics, Speech and Signal Processing, Las Vegas, Nevada, USA, 2008, pp. 1309–1312.
- [32] T. Wan, N. Canagarajah, and A. Achim, *Segmentation-driven image fusion based on alpha-stable modeling of wavelet coefficients*, IEEE Trans. Multimedia 11(4) (2009) pp. 624–633.
- [33] Z. Wang and A. Bovik, *A universal image quality index*, Signal Process. Lett. 9(3) (2002), pp. 81–84.
- [34] Z. Wang, D. Ziou, C. Armenakis, D. Li, and Q. Li, *A comparative analysis of image fusion methods*, IEEE Trans. Geosci. Remote Sens. 43(6) (2005), pp. 1391–1402.
- [35] A. Wang, H. Sun, and Y. Guan, *The application of wavelet transform to multi-modality medical image fusion*, Proceedings of the IEEE Conference on Networking, Sensing and Control, Ft. Lauderdale, Florida, USA, 2006, pp. 270–274.